

Theoretical design of single-molecule NOR and XNOR logic gates by using transition metal dibenzotetraaza[14]annulenes

Zi-Qun Wang(王子群), Fei Tang(唐菲), Mi-Mi Dong(董密密), Ming-Lang Wang(王明郎), Gui-Chao Hu(胡贵超), Jian-Cai Leng(冷建材), Chuan-Kui Wang(王传奎), Guang-Ping Zhang(张广平)

Citation: Chin. Phys. B . 2020, 29(6): 067202 . **doi:** 10.1088/1674-1056/ab84cf
Journal homepage: http://cpb.iphy.ac.cn; http://iopscience.iop.org/cpb

What follows is a list of articles you may be interested in

Electrically tunable spin diode effect in a tunneling junction of quantum dot

Xukai Peng(彭许凯), Zhengzhong Zhang(张正中)

Chin. Phys. B . 2019, 28(12): 127202 . **doi:** 10.1088/1674-1056/ab53d0

Recent spinterfacial studies targeted to spin manipulation in molecular spintronic devices

Xian-Rong Gu(谷现荣), Li-Dan Guo(郭立丹), Xiang-Nan Sun(孙向南)

Chin. Phys. B . 2018, 27(10): 107202 . **doi:** 10.1088/1674-1056/27/10/107202

Spin transport in a chain of polygonal quantum rings with Dresselhaus spin-orbit coupling

Han-Zhao Tang(唐翰昭), Xiao-Teng Yao(要晓腾), Jian-Jun Liu(刘建军)

Chin. Phys. B . 2017, 26(11): 117203 . **doi:** 10.1088/1674-1056/26/11/117203

Weak antilocalization and interaction-induced localization of Dirac and Weyl Fermions in topological insulators and semimetals

Hai-Zhou Lu(卢海舟), Shun-Qing Shen(沈顺清)

Chin. Phys. B . 2016, 25(11): 117202 . **doi:** 10.1088/1674-1056/25/11/117202

Control of Hall angle of Skyrmion driven by electric current

Gao-Bin Liu(刘高斌), Da Li(李达), de Chatel P F, Jian Wang(王健), Wei Liu(刘伟), Zhi-Dong Zhang(张志东)

Chin. Phys. B . 2016, 25(6): 067203 . **doi:** 10.1088/1674-1056/25/6/067203

Theoretical design of single-molecule NOR and XNOR logic gates by using transition metal dibenzotetraaza[14]annulenes*

Zi-Qun Wang(王子群)[1], Fei Tang(唐菲)[1], Mi-Mi Dong(董密密)[1], Ming-Lang Wang(王明郎)[1], Gui-Chao Hu(胡贵超)[1], Jian-Cai Leng(冷建材)[2], Chuan-Kui Wang(王传奎)[1,†], and Guang-Ping Zhang(张广平)[1,‡]

[1] *Shandong Key Laboratory of Medical Physics and Image Processing & Shandong Provincial Engineering and Technical Center of Light Manipulations, School of Physics and Electronics, Shandong Normal University, Jinan* 250358, *China*

[2] *Department of Physics, School of Electronic and Information Engineering, Qilu University of Technology (Shandong Academy of Sciences),Jinan* 250353, *China*

(Received 1 January 2020; revised manuscript received 19 March 2020; accepted manuscript online 31 March 2020)

The idea of replacing traditional silicon-based electronic components with the ones assembled by organic molecules to further scale down the electric circuits has been attracting extensive research focuses. Among the molecularly assembled components, the design of molecular logic gates with simple structure and high Boolean computing speed remains a great challenge. Here, by using the state-of-the-art nonequilibrium Green's function theory in conjugation with first-principles method, the spin transport properties of single-molecule junctions comprised of two serially connected transition metal dibenzotetraaza[14]annulenes (TM(DBTAA), TM = Fe, Co) sandwiched between two single-walled carbon nanotube electrodes are theoretically investigated. The numerical results show a close dependence of the spin-resolved current-voltage characteristics on spin configurations between the left and right molecular kernels and the kind of TM atom in TM(DBTAA) molecule. By taking advantage of spin degree of freedom of electrons, NOR or XNOR Boolean logic gates can be realized in Fe(DBTAA) and Co(DBTAA) junctions depending on the definitions of input and output signals. This work proposes a new kind of molecular logic gates and hence is helpful for further miniaturization of the electric circuits.

Keywords: single-molecule junction, molecular logic gate, spin transport, nonequilibrium Green's function method

PACS: 72.25.–b, 85.65.+h, 85.75.–d **DOI:** 10.1088/1674-1056/ab84cf

1. Introduction

Logic gates, which can take single- or two-input signals and then generate a binary output signal, are elementary blocks of extensively used digital integrated circuits. Enhancing the circuit integration by scaling down the electronic components can effectively improve the performance of integrated circuits. On the other hand, as the traditional electronic components are continually approaching to nano or even sub-nano scale, further miniaturization of silicon-based electronic components faces extremely formidable challenges due to limitations in current processing technology and prominent influence of quantum effect. As one of promising solutions, utilizing molecules as building blocks to design functional electronic devices, which are potential candidates to substitute traditional silicon-based components, has been drawing a great deal of research attention.[1–4] So far, as a result of advances in experimental approaches and theoretical methods,[5–8] a large number of functional molecular devices have been successfully designed and synthesized, such as molecular wires,[9,10] molecular rectifiers,[11–13] molecular transistors,[14,14] molecular sensors,[16,17] and molecular switches.[18–21] However, assembly of logic gates from these molecular device still encounters huge difficulties since there is lack of mature integration approaches in the field of molecular electronics. On the contrary, the idea of directly using a single molecule or a set of combined molecules to design logic gates has been put forward and lots of works have demonstrated its feasibility.[22–26] For example, using a dithienylethene molecule as the functional kernel, Meng *et al.* have realized two-input OR and three-input AND-OR single-molecule logic gates, which take optical and electrochemical stimuli as input signals.[22] Zhang *et al.* have fabricated an AND single-molecule logic gate by two serially connected molecular kernels, of which the conductance can be controlled by illumination and pH, respectively.[23] Nevertheless, a common issue for the above synthesized molecular logic gates is that the Boolean computing relies on changes of geometric structures of functional molecular kernels induced by the switch of input signals. This will take considerable time and thus cause delayed response of output signals.

Spin degree of freedom is an important intrinsic property for electrons. The ability of controlling transport behavior of electron spin provides a significant way to develop high-performance electronic components.[27–34] Naturally, electron

*Project supported by the National Natural Science Foundation of China (Grant Nos. 11874242, 21933002, and 11704230), China Postdoctoral Science Foundation (Grant No. 2017M612321), and the Taishan Scholar Project of Shandong Province of China.

†Corresponding author. E-mail: ckwang@sdnu.edu.cn

‡Corresponding author. E-mail: zhangguangping@sdnu.edu.cn

© 2020 Chinese Physical Society and IOP Publishing Ltd

spin can also be utilized in designing molecular logic gates. Specifically, input/output signals of a logic gate can be carried by electron spin (i.e., spin-up and spin-down). In this case, fast switch of the spin of electrons under external fields (e.g., magnetic field) enables high-speed Boolean computing. Taking advantage of this concept, a few single-molecule logic gates based on spin degree of freedom of electrons have been designed.[35–37] Recently, by connecting manganese phthalocyanine molecules to carbon nanotube electrodes with different connection manners, Zhao *et al.* have put forward three molecular logic gates, where NOT, AND, and OR Boolean operations can be realized.[35] Meanwhile, Zeng *et al.* have proposed an easy approach to achieve AND molecular logic gates by covalently merging magnetic transition metal porphyrin molecules into the edges of a graphene nanoribbon.[36] Differently, by defining the thermal-induced spin-down current as the output signal, Gao *et al.* have also demonstrated that an AND logic gate can be achieved in manganese-oligoporphyrin based molecular junction, which is driven by temperature difference instead of bias voltage on the left and right electrodes.[37]

As another intriguing organic macrocyclic compound, dibenzotetraaza[14]annulene (denoted DBTAA) is now attracting more and more focuses. Similar to porphyrin molecule, a series of transition metal atoms (TMs) can be accommodated in the cavity of DBTAA molecules, endowing this tetradentate compound with different magnetic properties.[38,39] In 2015, Wu *et al.* built single-molecule junctions composed of TM(DBTAA) molecules sandwiched between two zigzag graphene nanoribbons and investigated the corresponding spin-dependent transport properties. Perfect spin-filtering effect can be observed for junctions with Fe(DBTAA) molecules.[40] More recently, using carbon atomic chains (CACs) to connect two Fe(DBTAA) molecules, Zeng *et al.* have found spin-filtering efficiency and magnetoresistance fluctuate against odd and even number of carbon atoms in the CACs.[41] These works demonstrate that TM(DBTAA) molecules can effectively generate spin polarized current in a single-molecule device and are promising candidates for designing molecular logic gates. In this work, we have constructed single-molecule junctions by sandwiching two serially connected TM(DBTAA) (TM = Fe, Co) molecules between (4,4) single-walled carbon nanotube (SWCNT) electrodes via CACs. Spin-resolved electron transport properties of these single-molecule junctions under parallel- and antiparallel-spin polarizations for the two TM(DBTAA) molecular kernels are theoretically investigated. Based on calculated spin-resolved current–voltage (I–V) curves, it is revealed that Fe(DBTAA) and Co(DBTAA) junctions can act as NOR or XNOR molecular logic gates relying on the definitions of the output signal. In the following parts of this article, theoretical model and computational details are given in Section 2. Numerical results and discussion are presented in Section 3. Finally, a conclusion is given in Section 4.

2. Theoretical model and computational details

Schematic illustration of the studied single-molecule junctions is depicted in Fig. 1. The junction can be divided into three parts: the left electrode (marked by red rectangle), the right electrode (marked by blue rectangle), and the central region. Nonmagnetic metallic (4,4) SWCNTs are adopted as electrodes.[35] Dangling bonds at the open end of each SWCNT electrode are passivated by hydrogen atoms. The central region is comprised of two serially connected magnetic TM(DBTAA) molecules sandwiched between two SWCNTs through CACs, which have been recently fabricated experimentally[42] and widely used to bridge organic molecules and electrodes in theoretical works.[43–45] All the CACs used in our study are in the form of polyyne with alternating single and triple bonds (see Table S1 and Fig. S1 in the Supporting Information), which is in agreement with the previous studies.[38,46,47] As each junction studied here contains two TM(DBTAA) molecules, there are two spin configurations for the two TM atoms. That is, for one case, the left and right TM atoms are parallel-spin polarized (denoted as P spin configuration). For the other case, the right TM atom is antiparallel-spin polarized with respected to the left one (denoted as AP spin configuration). In our study, two kinds of TM atoms, i.e., Fe and Co atoms, are considered. Therefore, there are four junctions in total in our investigation, which are respectively named as TM(DBTAA)-P/AP with TM = Fe and Co.

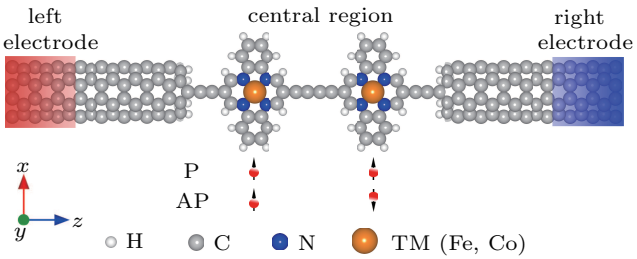


Fig. 1. Schematic of investigated single-molecule junctions consisting of two serially connected TM(DBTAA) (TM = Fe, Co) molecules embedded between two (4,4) SWCNT electrodes by CACs. The left and right electrodes are indicated by red and blue rectangles, respectively. P (AP) represents parallel-spin (antiparallel-spin) polarization of TM atoms under some external stimulations (e.g., magnetic field).

The geometric structures of the constructed molecular junctions are first optimized in Atomistix ToolKit package (ATK).[49,50] A 15 Å vacuum is applied along the x, y, and z directions of the central region to eliminate spurious interaction from neighboring images during optimization stage. Each atom is not relaxed until the residual force is less

than 0.05 eV/Å. The subsequent calculations of spin transport properties of each junction are also implemented in ATK by using the state-of-the-art nonequilibrium Green's function (NEGF) method in combination with density functional theory (DFT).[8] In our calculations, the spin-polarized generalized gradient approximation (SGGA) with the Perdew–Burke–Ernzerhof (PBE) parameterization is used for the exchange-correlation functional. A 200 Ryd energy cutoff is employed to determine real space grids and a double-ζ polarized (DZP) basis set is chosen to expand valence-electron wavefunctions. A $1\times1\times100$ k-point sampling in the Brillouin zone is utilized for the electrode calculations. The spin-resolved current is calculated according to the Landauer–Büttiker formula[51]

$$I_\sigma = \frac{e}{h}\int T_\sigma(E,V)[f(E-\mu_{\rm L})-f(E-\mu_{\rm R})]{\rm d}E, \qquad (1)$$

where σ represents spin-up ($\uparrow$) or spin-down ($\downarrow$) electrons; $f(E-\mu_{\rm L/R})$ is the Fermi-Dirac distribution function for electrons at energy E in the left/right electrode and $\mu_{\rm L/R}=E_{\rm F}\mp\frac{eV}{2}$ is chemical potential of the left/right electrode when a bias voltage V is applied to two electrodes. Herein, Fermi energy $E_{\rm F}$ is set to be zero. $T_\sigma(E,V)$ is spin-resolved transmission spectrum for spin-σ electrons, which is defined as

$$T_\sigma(E,V)={\rm Tr}[\Gamma_{\sigma,{\rm L}}(E,V)G_\sigma(E,V)\Gamma_{\sigma,{\rm R}}(E,V)G^\dagger_\sigma(E,V)], \qquad (2)$$

where $G_\sigma(E,V)$ is the retarded Green's function of the central region, and $\Gamma_{\sigma,{\rm L/R}}(E,V)$ indicates coupling strength between the left/right electrode and the central region.

3. Results and discussion

The Mulliken population of spin-up and spin-down electrons for the left and right TM atoms and total energies of TM(DBTAA)-P/AP junctions are shown in Table 1. For each TM(DBTAA)-P junction, both the left and right TM atoms have nearly the same population for either of two spin components. While for each TM(DBTAA)-AP junction, the population of spin-up and spin-down electrons for the right TM atom reverses compared to that in TM(DBTAA)-P junction. Therefore, spin population (the difference between population of spin-up and spin-down electrons) for the left and right TM atom is nearly the same for P spin configuration, but it has an opposite sign for AP spin configuration. In addition, the energies of the TM(DBTAA) junction are almost the same for the P and AP spin configurations. This suggests that the coupling between the left and right TM atoms is very weak. The coupling strength between the left and right TM atoms is evaluated to be about 0.028 eV for Fe(DBTAA) while about 0.024 eV for Co(DBTAA) according to the PDOS peak split at around 0.53 eV for Fe(DBTAA)-P junction and that at around 0.30 eV for Co(DBTAA)-P junction (see Fig. S2 in the Supporting Information).

Table 1. The Mulliken population of spin-up ($\uparrow$) and spin-down ($\downarrow$) electrons for the left and right TM atoms (respectively denoted $\rm TM_L$ and $\rm TM_R$) and total energies (in units of eV) of TM(DBTAA)-P/AP junctions, where TM = Fe, Co.

		$\rm TM_L$			$\rm TM_R$			Total energy
		$\uparrow$	$\downarrow$	$\uparrow-\downarrow$	$\uparrow$	$\downarrow$	$\uparrow-\downarrow$	
Fe(DBTAA)	P	4.939	2.831	2.108	4.940	2.831	2.109	−36739.17202
	AP	4.939	2.832	2.107	2.831	4.940	−2.109	−36739.17280
Co(DBTAA)	P	4.864	3.979	0.885	4.863	3.981	0.882	−37084.57563
	AP	4.864	3.979	0.885	3.981	4.863	−0.882	−37084.57554

The spin-resolved current–voltage (I–V) curves for TM(DBTAA) molecular junctions under P and AP spin configurations are investigated in the bias region of [−0.5 V, 0.5 V] and are displayed in Fig. 2. For Fe(DBTAA)-P as shown in Fig. 2(a1), one can hardly see any spin-up current within the bias range, while spin-down current rises up first, reaching 32.6 nA at 0.4 V and then goes down slightly. Obviously, only spin-down electrons are allowed to flow through the Fe(DBTAA)-P junction. When it turns to AP spin configuration, as presented in Fig. 2(a2), both the spin-up and spin-down currents are blocked in the whole studied bias range. This suggests that the change of spin configurations in Fe(DBTAA) junction effectively switches spin-down conducting state between ON and OFF. For the Co(DBTAA) junction, effect of changing spin configurations on the spin-resolved I–V curves (see Fig. 2(b)) is similar to the case of Fe(DBTAA) junctions. As shown in Fig. 2(b1), for P spin configuration, spin-up current can be completely ignored while spin-down current increases slowly from 0.0 V to 0.3 V and then rapidly soars up after 0.3 V, reaching a maximum value of about 1.9 μA at 0.5 V. For I–V curves of the Co(DBTAA)-AP junction shown in Fig. 2(b2), neither spin-up nor spin-down electrons can tunnel through the junction. Therefore, the junction switches to OFF conducting state for any spin electrons. One can note that in addition to the different profiles of the spin-down I–V curves for Co(DBTAA)-P and Fe(DBTAA)-P, the spin-down current for Co(DBTAA)-P is much larger than that for Fe(DBTAA)-P. This indicates that the features of the spin-resolved I–V curve (especially for the spin-down current under P spin configuration) is closely related to the TM atoms.

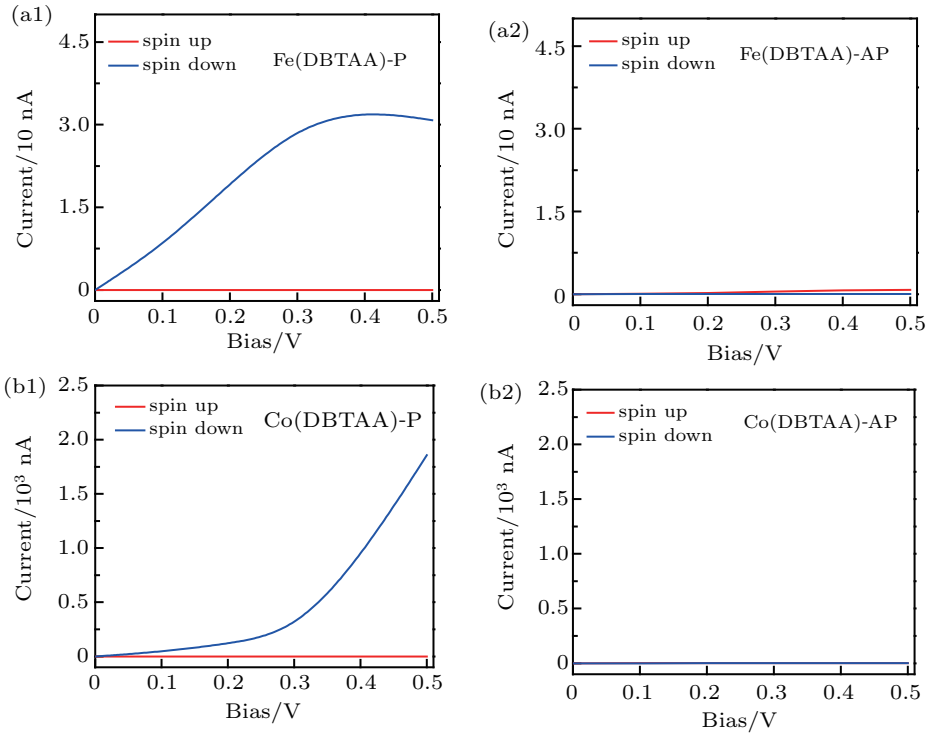


Fig. 2. Spin-dependent *I*–*V* curves for (a) Fe(DBTAA) and (b) Co(DBTAA) molecular junctions under P and AP spin configurations.

From the above discussion, it is easy to find that spin-down current of the investigated TM(DBTAA) junctions can be switched between ON and OFF states by manipulating the spin configurations of the two TM atoms. Such response of spin current to spin configurations in the junctions has a potential for realizing logic operations. From this viewpoint, it is worthy to inspect if the designed TM(DBTAA) junctions can act as logic gates. For this, we assume the spin polarization of the left and right TM(DBTAA) molecules in the junction as input signal, where spin-down and spin-up polarizations of the TM atom are defined as 0 and 1, respectively. Meanwhile, the low and high levels of spin-up current at 0.5 V are respectively used to represent output signals 0 and 1. According to the above definition for the input and output signals, the truth table for Fe(DBTAA) and Co(DBTAA) junctions is consequently obtained and presented in Table 2. Specifically, when Fe(DBTAA) junction is under P spin configuration, the corresponding input signals are [1,1], and then low spin-up current in *I*–*V* curves (see Fig. 2(a1)) indicates the output signal is 0. When it goes to AP configuration, Fig. 2(a2) shows two input signals are [1,0] and the output signal is also 0. When spin polarization of the left and right Fe atom is simultaneously reversed, owing to geometric symmetry of the junction, spin-up and spin-down *I*–*V* curves in Fig. 2 will exchange their roles. Therefore, for Fe(DBTAA) junction, the output signal will change to be 1 for a combination of input signals [0,0] (i.e., both the left and right TM atoms are spin-down polarized) while it will be still 0 for input signals [0,1] (i.e., the left TM atom is spin-down polarized but the right one is spin-up polarized). Finally, only input signals [0,0] generate an output signal of 1 in Fe(DBTAA) junction, which suggests a NOR Boolean logic function. Similarly, Co(DBTAA) junction also works as a NOR logic gate as shown in Table 2.

Table 2. Truth table for TM(DBTAA) (TM = Fe, Co) junctions as logic gates, where input signals are defined by spin polarization of the left and right TM atoms and output signals are defined by the spin-up current.

Input: 0 = TM (↓); 1 = TM (↑) Output: 0 = low $I_{\uparrow}$; 1 = high $I_{\uparrow}$				
	Input 1	Input 2	Output	Logic gate
Fe(DBTAA)	1	1	0	NOR
	1	0	0	
	0	1	0	
	0	0	1	
Co(DBTAA)	1	1	0	NOR
	1	0	0	
	0	1	0	
	0	0	1	

In fact, one junction may realize different Boolean logic functions by adopting different definitions of input and output signals. Table 3 exhibits the truth table for the investigated junctions when total current instead of spin-up current is taken as output signal. Here, for a specified bias voltage, e.g., 0.5 V, a low total current represents output signal 0 while a high one indicates output signal 1. For Fe(DBTAA) and Co(DBTAA) junctions, the plots of total current versus voltage (see Fig. S3 in the Supporting Information) show that high total current can always be observed for both [1,1] and [0,0] input signals (i.e. the spin polarization of the left and right TM atoms is parallel), which indicates output signal is 1. For [1,0] and [0,1]

input signals (i.e., the spin polarization of the left and right TM atoms is antiparallel), the total current is severely blocked resulting in output signal 0. Therefore, both Fe(DBTAA) and Co(DBTAA) junctions can work as XNOR logic gate.

Table 3. Truth table for TM(DBTAA) (TM = Fe, Co) junctions as logic gates, where input signals are defined by spin polarization of the left and right TM atoms and output signals are defined by the total current.

Input: 0 = TM (↓); 1 = TM (↑) Output: 0 = low I_{total}; 1 = high I_{total}				
	Input 1	Input 2	Output	Logic gate
Fe(DBTAA)	1	1	1	XNOR
	1	0	0	
	0	1	0	
	0	0	1	
Co(DBTAA)	1	1	1	XNOR
	1	0	0	
	0	1	0	
	0	0	1	

The above discussion suggests that the spin-dependent electron transport properties of the investigated junctions are closely related to the kinds of embedded TM atoms and their spin configurations. In order to relate the spin-resolved *I*–*V* curves of the TM(DBTAA) junctions to TM atoms and their spin configurations, spin-dependent transmission spectra for each junction have been explored, as shown in Fig. 3. As shown in Fig. 3(a1), transmission spectra for the Fe(DBTAA)-P junction show no observable spin-up transmission coefficient in the energy range of [−0.6 eV, 0.6 eV] at 0 V, which leads to the block of spin-up current in the whole studied bias voltage range. On the contrary, a broad spin-down transmission peak can be found at −0.25 eV under zero bias voltage. Meanwhile, a bimodal spin-down transmission peak is found above E_F with the energy-lower peak at 0.51 eV and the energy-higher one at 0.56 eV. When the bias is applied to the junction, the energy-higher peak moves away from E_F while the energy-lower one approaches to E_F (the detailed evolution of this bimodal transmission peak under bias voltage is given in Fig. S4 in the Supporting Information). However, the energy-lower transmission peak is yet not included in the bias window under 0.5 V. Although the spin-down transmission peak at −0.25 eV under 0.0 V shifts downwards away from E_F and the intensity of this transmission peak is lowered, the tail of this transmission peak can be included in the bias window as the bias voltage increases, contributing a clear spin-down non-resonant tunneling current. For Fe(DBTAA)-AP junction displayed in Fig. 3(a2), all the transmission peaks at 0.0 V observed in Fe(DBTAA)-P junction nearly vanish. Thus, transport channels for both spin-up and spin-down electrons are completely prohibited.

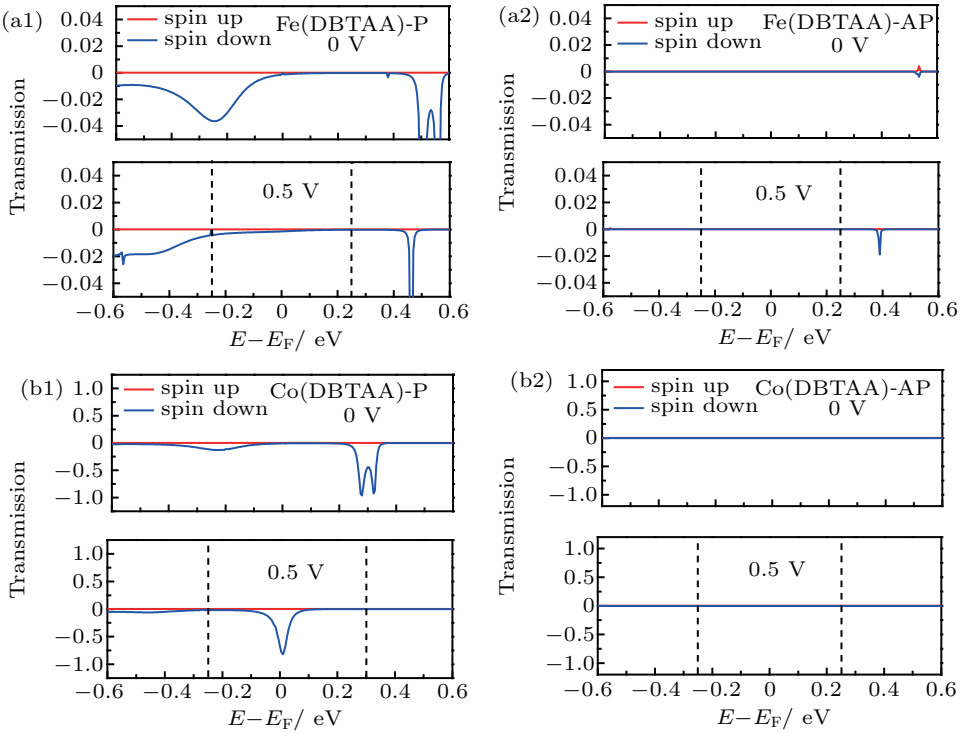


Fig. 3. Spin-dependent transmission spectra for (a) Fe(DBTAA)-P/AP and (b) Co(DBTAA)-P/AP junctions at 0 V and 0.5 V. The dashed lines denote the bias window.

When it turns to Co(DBTAA) junctions, as shown in Fig. 3(b), one can find the profiles of transmission spectra for Co(DBTAA)-P (Co(DBTAA)-AP) junction are pretty similar to those for Fe(DBTAA)-P (Fe(DBTAA)-AP) junction at 0.0 V. Specifically, as shown in Fig. 3(b1), there are also a spin-down transmission peak at around −0.25 eV and a bimodal spin-down transmission peak above E_F for Co(DBTAA)-P junction. At the same time, there is also no

visible transmission peak for both spin-up and spin-down electrons for Co(DBTAA)-AP junction as displayed in Fig. 3(b2). Differently, the bimodal spin-down transmission peak for Co(DBTAA)-P at 0.0 V is about 0.22 eV closer to E_F in comparison to the counterpart for Fe(DBTAA)-P. This leads to the energy-lower peak of the bimodal transmission peak be included in the bias window under a moderate bias voltage (the detailed evolution of this bimodal transmission peak under bias voltage is given in Fig. S5 in the Supporting Information), which is the dominated contribution to the spin-down current of Co(DBTAA)-P. Therefore, different charge transport mechanisms in Fe(DBTAA)-P and Co(DBTAA)-P junctions have been revealed. That is to say, the electronic transport for Fe(DBTAA)-P junction is in the non-resonant regime and is dominated by spin-down holes while the electronic transport for Co(DBTAA)-P junction is in the resonant regime and is contributed from spin-down electrons. That is why spin-down current through Co(DBTAA)-P junction is much larger than that through Fe(DBTAA)-P junction.

Origins of the spin-resolved transmission peaks around E_F are further rationalized by the spin-resolved PDOS, where the contributions of the left and right TM(BDTAA) molecules to the total DOS under zero bias voltage are analyzed. Also, spin-resolved frontier molecular orbitals obtained by molecular projected self-consistent Hamiltonian (MPSH) analysis are inspected to understand the contributions of spin electronic states to electron tunneling channels. From Fig. 4, one can find that for each spin component, the profiles of PDOS for the left and right molecular kernels in TM(DBTAA)-P are identical, which come from the degenerated electronic states dominated respectively by the left and right TM(DBTAA) molecules. Hybrid between the degenerated electronic states is in favor of forming electron tunneling channels. This can be inspected by exploring the spatial distributions of MPSH states around E_F for each TM(DBTAA) junction, which are shown in Fig. 5. For example, for Fe(DBTAA)-P junction in Fig. 4(a1), the spin-up electronic states at about 0.17 eV originate from spin-up LUMO (at 0.037 eV) and LUMO+1 (at 0.048 eV), which are respectively only localized on the right and left Fe(DBTAA) molecules as shown in Fig. 5(a1), impeding the formation of any tunneling channel for spin-up electrons around this energy. On the other hand, the spin-down electronic states at around −0.23 eV are contributed by spin-down HOMO (at −0.260 eV) and HOMO-1 (at −0.284 eV). Delocalized spatial distributions of spin-down HOMO and HOMO-1 (see Fig. 5(a1)) connect the left and right parts of the junction, contributing to a broad spin-down transmission peak at −0.25 eV as seen in Fig. 3(a1). Similarly, by the MPSH and PDOS analyses, one can also easily understand why the sharp spin-down PDOS at around 0.38 eV (dominated by spin-down LUMO and LUMO+1) contributes no transmission peaks while the bimodal spin-down PDOS at around 0.5 eV (contributed by spin-down LUMO+2 and LUMO+3) gives a bimodal transmission peak. For Co(DBTAA)-P junction, as seen in Figs. 4(b1) and 5(b1), the spin-down PDOS peaks below E_F are the superposition of delocalized states at around −0.23 eV (originating from spin-down HOMO-2 and HOMO-3) and localized ones at around −0.2 eV (originating from spin-down HOMO and HOMO-1). Therefore, one can conclude that the spin-down transmission peak at −0.23 eV in Fig. 3(b1) is from the spin-down HOMO-2 and HOMO-3. Meanwhile, by inspecting the spatial distributions of the wavefunctions shown in Fig. 5(b1), one can find that the bimodal spin-down PDOS at around 0.30 eV originates from the spin-down LUMO and LUMO+1 and these two electronic states contribute a bimodal transmission peak as seen in Fig. 3(b1). However, the spin-up LUMO and LUMO+1, which give rise to the PDOS peak at around 0.16 eV, hardly contribute the transmission peak due to their localized spatial distributions.

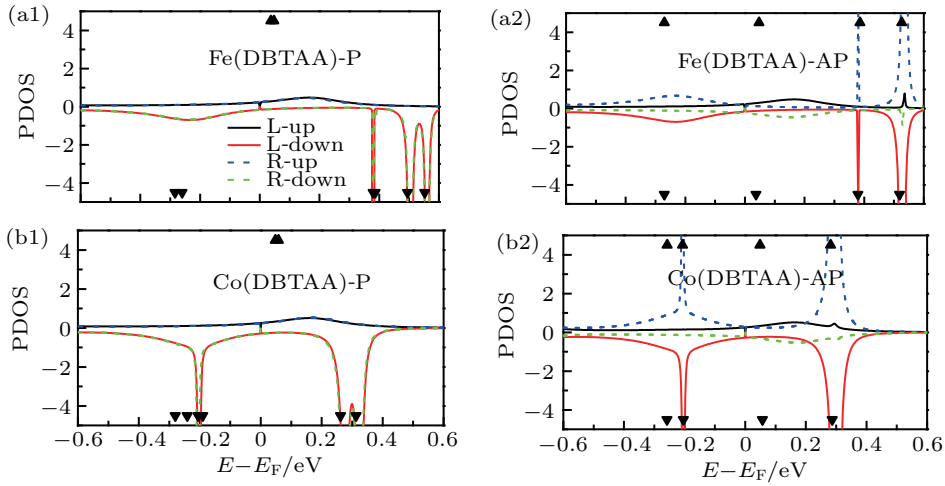


Fig. 4. Spin-resolved PDOS of the left (labeled as L) and right (labeled as R) TM(BDTAA) molecules for (a) Fe(DBTAA) and (b) Co(DBTAA) junctions under P and AP spin configurations at zero bias voltage. The black triangles denote the spin-resolved eigenvalues of frontier molecular orbitals obtained by MPSH analysis.

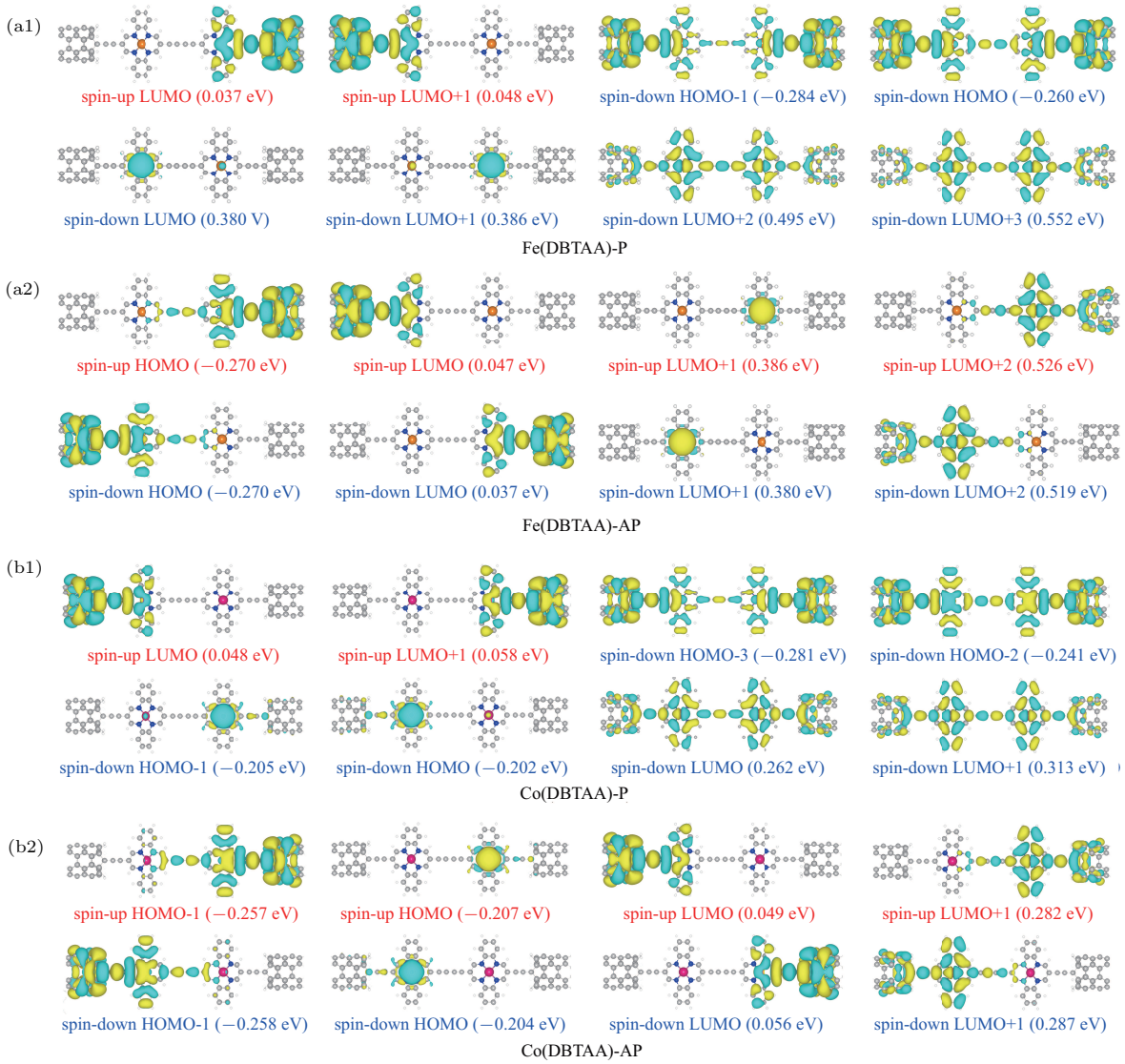


Fig. 5. Spatial distributions of frontier molecular orbitals for each TM(BDTAA) junction with P and AP spin configurations.

When the spin polarization of the right TM atom reverses and spin configuration turns to be antiparallel, it is clearly seen from Figs. 4(a2) and 4(b2) that the degeneracy between electronic states of the left and right TM(DBTAA) molecules for each spin component is eliminated and the spin-up (spin-down) PDOS of the right TM(DBTAA) molecule under P spin configuration reverses to spin-down (spin-up) branch under AP spin configuration. It means that, at a given energy, if PDOS is completely spin-polarized under P spin configuration, it would turn to be totally spin non-polarized under AP spin configuration since a spin-up electronic state and a counterpart spin-down one with the same energy respectively localize on the left and right TM(DBTAA) molecules. In this case, tunneling across the junction for either spin-up or spin-down electrons at this energy is entirely forbidden. This can also be verified by spatial distributions of frontier molecular orbitals (see Figs. 5(a2) and 5(b2)) of Fe(DBTAA)-AP and Co(DBTAA)-AP junctions.

4. Conclusions

In summary, by using the DFT based NEGF method, spin transport properties of single-molecule junctions, which are comprised of two serially connected magnetic TM(DBTAA) (TM = Fe, Co) molecules embedded between two SWCNT electrodes, have been investigated for both P and AP spin configurations. The calculated results reveal that spin configurations and the kind of TM atoms play important roles in determining the *I*–*V* characteristics of TM(DBTAA) junctions. Specifically, the spin polarizations of the *I*–*V* curves for Fe(DBTAA) and Co(DBTAA) junctions are very similar for both P and AP configurations. That is, for P spin configuration, only spin-down electrons are allowed to flow through the junctions while spin-up ones are prohibited. For AP spin configuration, both spin-up and spin-down currents are blocked. Large spin-down current under P spin configuration stems from the delocalization of spin-down electronic states among two molecular kernels and the bridging CAC. However, when

it turns to AP spin configuration, both the spin-up and spin-down electronic states around E_F are localized due to the complete mismatch between electronic states of the left and right molecular kernels for each spin component. It is found that, under P spin configuration, when the TM atom changes from Fe to Co, the charge transport mechanism of the junction is transformed from non-resonant to resonant tunneling regime, therefore resulting in a much larger spin-down current for Co(DBTAA)-P than Fe(DBTAA)-P. This can be ascribed to the fact that the conducting channel above E_F is much more closer to E_F for Co(DBTAA)-P than for Fe(DBTAA)-P. More interestingly, by defining different input and output signal criteria, it is found that Fe(DBTAA) and Co(DBTAA) junctions can work as NOR or XNOR molecular logic gate. Our work here proposes a new kind of molecular logic gates by taking advantage of the spin degree of freedom of electrons, which is helpful for further miniaturizing the electric circuits.

Supplementary data related to this article can be found in the Supporting Information.

References

[1] Aviram A and Ratner M A 1974 *Chem. Phys. Lett.* **29** 277
[2] Xin N, Guan J, Zhou C, Chen X, Gu C, Li Y, Ratner M A, Nitzan A, Stoddart J F and Guo X 2019 *Nat. Rev. Phys.* **1** 211
[3] Xiang D, Wang X, Jia C, Lee T and Guo X 2016 *Chem. Rev.* **116** 4318
[4] Guo X 2018 *Molecular-Scale Electronics: Current Status and Perspectives* (Switzerland: Springer International Publishing)
[5] Xu B and Tao N J 2003 *Science* **301** 1221
[6] Liu R, Bi J J, Xie Z, Yin K, Wang D, Zhang G P, Xiang D, Wang C K and Li Z L 2018 *Phys. Rev. Appl.* **9** 054023
[7] Liu R, Wang C K and Li Z L 2016 *Sci. Rep.* **6** 21946
[8] Brandbyge M, Mozos J L, Ordejón P, Taylor J and Stokbro K 2002 *Phys. Rev. B* **65** 165401
[9] Shu C H, Liu M X, Zha Z Q, Pan J L, Zhang S Z, Xie Y L, Chen J L, Yuan D W, Qiu X H and Liu P N 2018 *Nat. Commun.* **9** 2322
[10] Yu J X, Hou Z W and Liu X Y 2015 *Chin. Phys. B* **24** 067307
[11] Chen X, Roemer M, Yuan L, Du W, Thompson D, del Barco E and Nijhuis C A 2017 *Nat. Nanotechnol.* **12** 797
[12] Wei M Z, Wang Z Q, Fu X X, Hu G C, Li Z L, Wang C K and Zhang G P 2018 *Physica E* **103** 397
[13] Fu H Y, Sun F, Liu R, Suo Y Q, Bi J J, Wang C K and Li Z L 2019 *Phys. Lett. A* **383** 867
[14] Tans S J, Verschueren A R M and Dekker C 1998 *Nature* **393** 49
[15] Meng L, Xin N, Hu C *et al.* 2019 *Nat. Commun.* **10** 1450
[16] Li Z L, Bi J J, Liu R, Yi X H, Fu H Y, Sun F, Wei M Z and Wang C K 2017 *Chin. Phys. B* **26** 098508
[17] He Y, Zhang J and Zhao J 2014 *J. Phys. Chem. C* **118** 18325
[18] Wang Z Q, Wei M Z, Dong M M, Hu G C, Li Z L, Wang C K and Zhang G P 2018 *J. Phys. Chem. C* **122** 17650
[19] Weckbecker D, Coto P and Thoss M 2017 *Nano Lett.* **17** 3341
[20] Zhang G P, Mu Y Q, Zhao J M, Huang H, Hu G C, Li Z L and Wang C K 2019 *Physica E* **109** 1
[21] Fu X X, Zhang L X, Li Z L and Wang C K 2013 *Chin. Phys. B* **22** 028504
[22] Meng F, Hervault Y M, Shao Q, Hu B, Norel L, Rigaut S and Chen X 2014 *Nat. Commun.* **5** 3023
[23] Zhang N, Lo W Y, Jose A, Cai Z, Li L and Yu L 2017 *Adv. Mater.* **29** 1701248
[24] Collier C, Wong E, Belohradský M, Raymo F, Stoddart J, Kuekes P, Williams R and Heath J 1999 *Science* **285** 391
[25] Erbas-Cakmak S, Kolemen S, Sedgwick A C, Gunnlaugsson T, James T D, Yoon J and Akkaya E U 2018 *Chem. Soc. Rev.* **47** 2228
[26] de Silva A P and Uchiyama S 2007 *Nat. Nanotechnol.* **2** 399
[27] Rocha A R, García-Suárez V M, Bailey S W, Lambert C J, Ferrer J and Sanvito S 2005 *Nat. Mater.* **4** 335
[28] Pati R, Senapati L, Ajayan P M and Nayak S K 2003 *Phys. Rev. B* **68** 100407
[29] Hu G C, Zhang Z, Li Y, Ren J F and Wang C K 2016 *Chin. Phys. B* **25** 057308
[30] Wan H, Zhou B, Chen X, Sun C Q and Zhou G 2012 *J. Phys. Chem. C* **116** 2570
[31] Gu X R, Guo L D and Sun X N 2018 *Chin. Phys. B* **27** 107202
[32] Zhang X W, Zhao H, Sang T, Liu X C and Cai T 2013 *Chin. Phys. Lett.* **30** 017201
[33] Qiu Z W and Hou D 2019 *Chin. Phys. B* **28** 088504
[34] Hao R, Zang R, Zhou T, Kan S, Yan S, Liu G, Han G, Yu S and Mei L 2019 *Chin. Phys. B* **28** 037202
[35] Zhao W, Zou D, Yang C L and Sun Z 2017 *J. Mater. Chem. C* **5** 8862
[36] Zeng J and Chen K Q 2018 *Phys. Chem. Chem. Phys.* **20** 3997
[37] Gao X J, Zhao P and Chen G 2018 *Org. Electron.* **62** 277
[38] Whyte A M, Shuku Y, Nichol G S, Matsushita M M, Awaga K and Robertson N 2012 *J. Mater. Chem.* **22** 17967
[39] Khaledi H, Olmstead M M, Mohd Ali H and Thomas N F 2013 *Inorg. Chem.* **52** 1926
[40] Wu Q H, Zhao P and Chen G 2015 *Org. Electron.* **25** 308
[41] Zeng J and Chen K Q 2016 *Carbon* **104** 20
[42] Rong Y and Warner J H 2014 *ACS Nano* **8** 11907
[43] Zeng M, Shen L, Cai Y, Sha Z and Feng Y 2010 *Appl. Phys. Lett.* **96** 042104
[44] Zanolli Z, Onida G and Charlier J C 2010 *ACS Nano* **4** 5174
[45] Wang B, Li J, Yu Y, Wei Y, Wang J and Guo H 2016 *Nanoscale* **8** 3432
[46] Khoo K H, Neaton J B, Son Y W, Cohen M L and Louie S G 2008 *Nano Lett.* **8** 2900
[47] Shen L, Zeng M, Yang S W, Zhang C, Wang X and Feng Y 2010 *J. Am. Chem. Soc.* **132** 11481
[48] Song Y, Xie Z, Zhang G P, Ma Y and Wang C K 2013 *J. Phys. Chem. C* **117** 20951
[49] Soler J M, Artacho E, Gale J D, García A, Junquera J, Ordejón P and Sánchez-Portal D 2002 *J. Phys.: Condens. Matter* **14** 2745
[50] Atomistix ToolKit, version 2015 1; QuantumWise A/S, https://quantumwise.com (accessed Dec. **31** 2019)
[51] Büttiker M, Imry Y, Landauer R and Pinhas S 1985 *Phys. Rev. B* **31** 6207